Colloidal Crystals

DOI: 10.1002/anie.201409878

Tuning the Colloidal Crystal Structure of Magnetic Particles by External Field**

*Antara Pal, Vikash Malik, Le He, Ben H. Erné, Yadong Yin, Willem K. Kegel, and Andrei V. Petukhov**

Abstract: *Manipulation of the self-assembly of magnetic colloidal particles by an externally applied magnetic field paves a way toward developing novel stimuli responsive photonic structures. Using microradian X-ray scattering technique we have investigated the different crystal structures exhibited by self-assembly of core–shell magnetite/silica nanoparticles. An external magnetic field was employed to tune the colloidal crystallization. We find that the equilibrium structure in absence of the field is random hexagonal close-packed (RHCP) one. External field drives the self-assembly toward a body-centered tetragonal (BCT) structure. Our findings are in good agreement with simulation results on the assembly of these particles.*

Magnetic nanoparticles have recently received a great deal of attention due to their unique colloidal, magnetic, and optical properties. They have been widely used in the material fabrication and design of functional devices in many fields, including imaging,[1] catalysis,[2] medicine,[3–5] and DNA separation.[6,7] The ability to manipulate the self-assembly of colloids by external tuning parameters such as magnetic or electric field, temperature, and concentration is essential to develop new stimuli-responsive materials. For instance, magnetic and electric field guided nanoparticles are being used to create superstructures, ranging from string fluids to crystalline phases.[8–15] This bottom up approach utilizes the fast, anisotropic, and reversible nature of the magnetic dipole–dipole interaction, which can either be attractive or repulsive in nature depending on the angle between the magnetic field and the line connecting the dipoles. The mere fact that a colloidal self-assembly can be tuned externally by a magnetic field has provided enormous flexibility as well as a wider scope for experimental design in diverse fields, for example, photonics,[16,17] drug delivery,[18,19] patterning,[20–24] and magnetic levitation.[25–28]

Silica-covered magnetite core–shell nanoparticles are of special interest because of their high yield and chemical properties. In particular, the ability of these magnetic particles to self-assemble in nonaqueous solutions allows us to fabricate field-responsive polymer composite films for potential applications as displays or sensors. The silica surface can be easily modified with a large variety of functional groups through silane chemistry to further broaden the choice of solvents as well as the applications. For example, a 1D assembly of these particles has been shown to exhibit tunable photonic properties.[29,30] A suspension of these nanoparticles displays colors in the visible range of the electromagnetic spectrum, which can be tuned by the particle size as well as by an external magnetic field.[31–33] Further, these core–shell particles can be used to fabricate humidity sensors and rewritable photonic paper and ink.[34–36]

To fully exploit the true potential of the super-paramagnetic magnetite colloidal nanoparticles in various applications one must fully address the fundamental questions that refer to their colloidal crystallization with and without a magnetic field. At this point only a handful of studies are reported in the literature along this direction. Simulations, that have tried to address these questions, predict an assortment of equilibrium phases such as the body-centered tetragonal (BCT) and face-centered cubic (FCC) phases that can coexist with the 1D particle chains.[37–40] Experimentally it has been shown that in the presence of a magnetic field these nanoparticles self-assemble to a 1D chain phase. With an increase of both the strength and the gradient of the applied magnetic field[29,41–43] these chains evolve into 2D sheets and 3D structures. However, to the best of our knowledge, neither an exact crystal structure nor a detailed in situ study of the variation of the crystalline phases with the strength of the magnetic field are available.

In the present study, we have used microradian X-ray scattering technique to investigate the different crystal structures exhibited by a self-assembly of core–shell magnetite/silica nanoparticles (size ~170 nm) both in the presence and absence of an external magnetic field (see the Supporting Information (SI) for a more detailed discussion of the materials and methods). A detailed analysis of the diffraction patterns indicates that in the absence of the magnetic field a random hexagonal closed-packed (RHCP) structure is

[*] Dr. A. Pal, Dr. B. H. Erné, Prof. Dr. W. K. Kegel, Dr. A. V. Petukhov
Van't Hoff Laboratory for Physical and Colloid Chemistry
Debye Institute for NanoMaterials Science, Utrecht University
Padualaan 8, 3584 CH, Utrecht (The Netherlands)
E-mail: a.v.petukhov@uu.nl
Dr. V. Malik
Physics Department, University of Wisconsin Milwaukee
1900 E. Kenwood Blvd., Milwaukee, Wisconsin 53211 (USA)
Dr. L. He, Prof. Dr. Y. Yin
Department of Chemistry, University of California Riverside
501 Big Springs Road, Riverside, California 92521 (USA)

[**] A.P. thanks The Netherlands Organization for Scientific Research (NWO; 700.10.355), V.M. thanks the Swiss National Science Foundation (SNF) for financial support (PBFRP2-134284), Y.Y. thanks for financial support from the U.S. National Science Foundation (DMR-0956081). The personnel of the DUBBLE beamline are thanked for their help with the synchrotron experiment, and NWO is thanked for granting beamtime.

Supporting information for this article is available on the WWW under http://dx.doi.org/10.1002/anie.201409878.

stabilized, whereas BCT is favored in the presence of a magnetic field. At low magnetic field strength (~12 mT), one observes the formation of 1D chains.[42] Vertical stripes observed in the diffraction pattern are a characteristic feature of this 1D assembly (Figure S2).

Figure 1 shows the scattering patterns obtained at a constant magnetic field strength $H = 26.5$ mT, for a fixed vertical position of the capillary ($z = 48$ mm) but by varying the angle

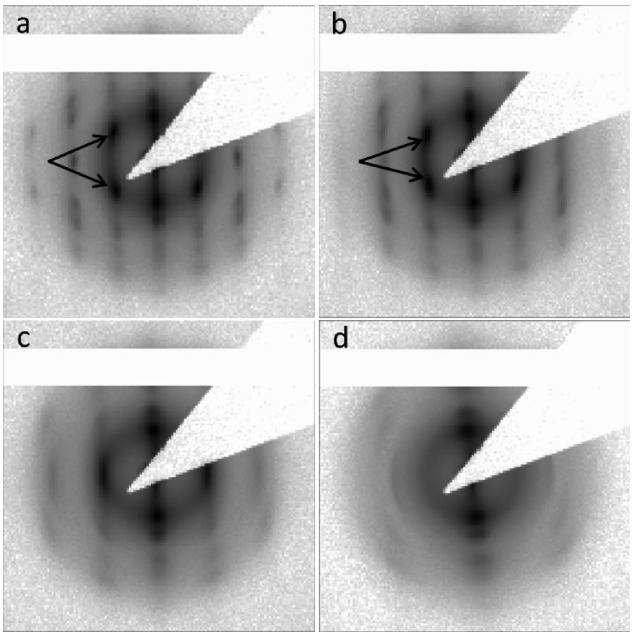

Figure 1. Angle (ϕ) dependence of scattering patterns obtained at a) $\phi = 0°$, b) $\phi = 20°$, c) $\phi = 40°$, and d) $\phi = 60°$; ϕ being the angle between the incident X-ray beam and the normal to the capillary walls. Here, magnetic field (H) and z-position were kept constant at $H = 26.5$ mT and $z = 48$ mm from the bottom of the capillary.

ϕ, which is defined as the angle between the incident X-ray beam and the normal to the capillary walls. Sharp reflections observed at angle $\phi = 0°$ indicate the presence of colloidal crystal. With the rotation of the capillary, reflections indicated by the arrows gradually start to move in the direction of increasing $|Q_x|$ and decreasing $|Q_y|$ (Figure 1 b). Q_x and Q_y are the respective components of the scattering vector taken along the direction of the magnetic field and perpendicular to it. Further, symmetric reflections at $+Q_y$ and $-Q_y$ collapse at $Q_y = 0$ and disappear at larger ϕ. Similar observations were made for the other higher order peaks. When the angle of rotation is increased to 40° only few reflections are observed because most of them seem to have now fused together at this value of ϕ, which can be seen in Figure 1 c. Finally, at $\phi = 60°$ only those reflections are observed that lie on the vertical axes with $Q_x = 0$, that is, reflections above and below the beam stop are visible (Figure 1 d). All these observations point toward the fact that each of these visible features does not correspond to a Bragg spot but is rather a part of a Bragg ring in the 3D reciprocal space. The spread and position of these visible features depend on the intersection of the Ewald sphere with a given Bragg ring. This seems to be quite plausible in the present case, because one of the crystallographic axes has been fixed by the applied magnetic field whereas the other two axes can be equally distributed in a plane perpendicular to the field. As a result, each Bragg spot becomes a ring in the Fourier space. This experimental observation leads us to the conclusion that this sample contains a texture of smaller crystallites with one of the crystallographic directions aligned along the magnetic field.

As has been mentioned earlier, the sample is no more a single crystal, rather it shows a quasi-powder diffraction pattern; effectively the diffraction pattern at normal incidence (Figure 1 a) should contain all the necessary information regarding the crystal structure. Figure 1 a gives an impression of a hexagonally arranged set of reflections. However, a closer look reveals that there are some additional features that do not fall onto a single hexagonal lattice. For instance, the first order peaks in the vertical direction (above and below the beam stop) is split with the strong satellites falling off the hexagonal lattice.

To figure out the exact crystal structure we have modeled the diffraction pattern by considering BCT and FCC crystal structures as the possible candidates. The cartoons in Figure 2 f and g show the real space unit cells of the BCT and FCC lattice, respectively. The BCT lattice results from squeezing a body-centered cubic lattice along one of its principal directions, so that the cube becomes a rectangular parallelepiped with a square base (of side a) and its height $c < a$. For this particular case, due to the strong dipole–dipole attraction, the nearest neighbor distance should be along the magnetic field making this direction to be a special one. If it is a BCT lattice, the axis ($\langle 001 \rangle$), which is different from the other two axes of the crystal, should align along that particular direction. In the FCC lattice, the particles are touching each other along the diagonal of each face of the cubes making the nearest neighbor distance along the $\langle 110 \rangle$ directions. If the crystal under consideration has an FCC structure, one of the $\langle 110 \rangle$ directions should be aligned along the magnetic field.

Let us consider the x axis of the laboratory coordinate system to coincide with the magnetic field. Since the relative orientation of the other two axes is equally probable, it is expected for all the reflections to spread over a circle of radius Q_y around the field direction. In the laboratory frame, however, one observes only those reflections that correspond to the wave vector $\mathbf{Q} \equiv (Q_x, Q_y, 0)$ with the z component equal to zero. Because the diffraction intensity is spread over a circle, the intensity of the visible reflection is proportional to Q_y^{-1}. An additional factor that affects the intensity and has to be taken into account is the multiplicity M of a reflection, which shows the number of times one can observe a reflection at the position $\mathbf{Q}$ if one rotates one single crystal by 360° around the x axis.

The relative intensity of a reflection can then be indicated by a quantity,

$$I \propto \frac{M}{Q_y}. \tag{1}$$

A closer look at Equation (1) immediately tells us that we hit a singularity for reflections having $Q_y = 0$, i.e., intensity

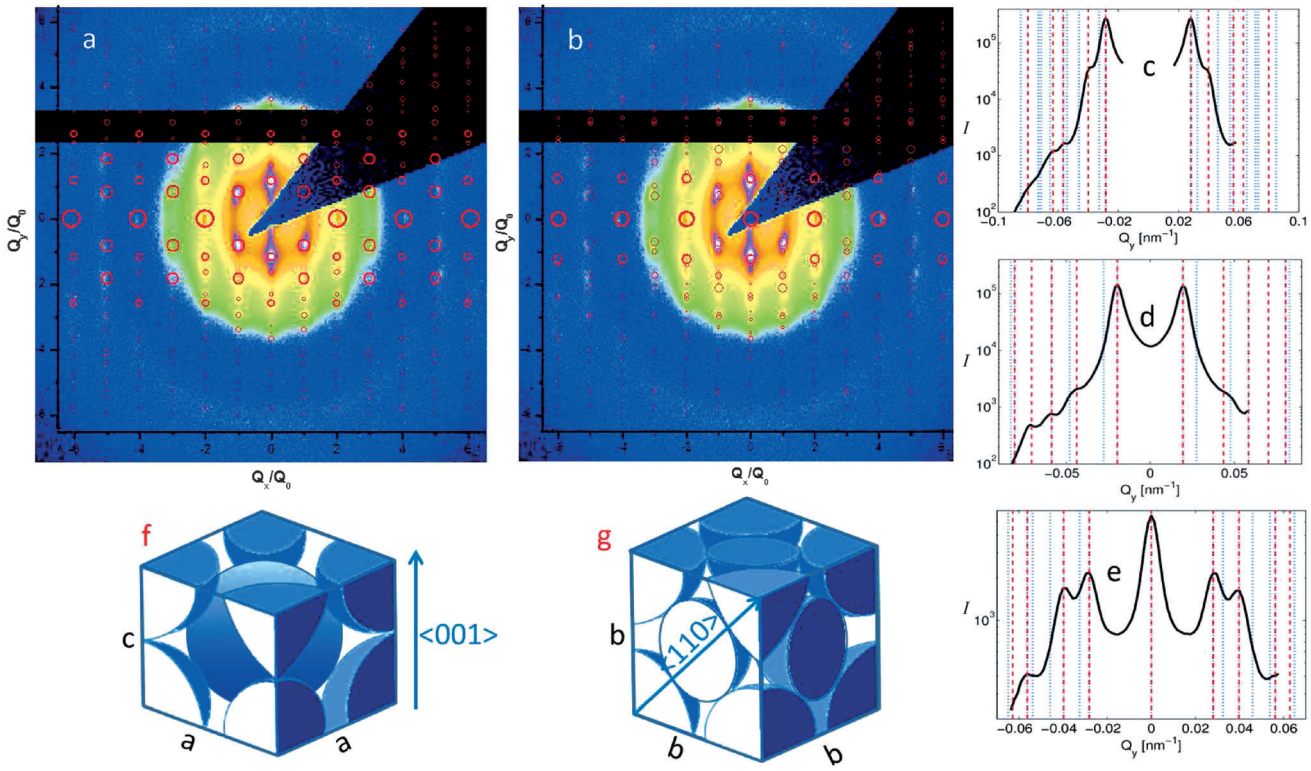

Figure 2. a,b) Diffraction pattern obtained at $z = 48$ mm, $\phi = 0°$, and magnetic field H = 26.5 mT, simulated reflections (red circles) from a) body-centered tetragonal (BCT) and b) face-centered cubic (FCC) crystals are superimposed over the scattering pattern. The external magnetic field is along Q_x. The simulated data is scaled with respect to a scaling parameter Q_0, which is related to the nearest-neighbor distance. c–e) Intensity (I) versus Q_y profiles taken at c) $Q_x = 0$, d) $Q_x = -Q_0$, and e) $Q_x = -2Q_0$. Red dashed lines represent the expected peak positions for a BCT crystal, whereas blue dotted ones show the peak positions for a FCC crystal. f,g) Real space unit cell of BCT and FCC lattices, respectively. In the BCT lattice, the nearest-neighbor distance is along the ⟨001⟩ direction, whereas that for FCC one is along the ⟨110⟩ direction.

corresponding to these reflections goes to ∞. In practice the intensity of reflections with $Q_y = 0$ is limited by several factors such as instrumental parameters, fluctuations in the orientation of the crystallographic x axis, and the crystal disorder that can broaden the peaks. Since the effect of these factors has not been incorporated in the model, we encounter singularity in the value of I for $Q_y = 0$. We have mapped those points with an arbitrarily high intensity value. It would be worthwhile to mention here that in our model we have exclusively considered the structure factor but not the form factor or the Debye–Waller factor.

The overlay of our models for BCT and FCC with the experimental scattering pattern is shown in Figure 2 a and b, respectively (for detailed analysis see SI). The simulated data is scaled with respect to a scaling parameter Q_0 which is related to the nearest-neighbor distance. The red circles represent the simulated reflections from the model. The relative sizes of the circles indicate the relative intensities I as calculated by using Equation (1). One can see that the BCT model is in remarkable agreement with the experimental diffraction pattern in Figure 2 a, whereas the correspondence in panel (b) with expected FCC peaks is poor.

Furthermore, we have plotted the experimental intensity profiles as a function of Q_y at three different values of Q_x namely, $Q_x = 0$, $Q_x = -Q_0$, $Q_x = -2Q_0$ as shown in (Figure 2 c–e), respectively. The red dashed lines represent the peak positions expected for a BCT crystal, whereas the blue dotted ones represent that for a FCC crystal. A close inspection of the plots shows that the red lines indeed pass through the experimental peak positions indicating the experimental peaks are appearing at the expected position for the BCT lattice, whereas the blue ones are not. This observation clearly points to the fact that the experimental crystal structure is BCT rather than FCC.

Surprisingly, the c/a ratio appeared to be 15% smaller than that of the typical value $c/a = \sqrt{2/3}$ as expected from touching spheres, c and a being 231 nm and 331.6 nm, respectively. This difference as well as the stability of the BCT lattice can be accounted for by the following argument. Self-assembly of silica/magnetite nanoparticles arises from a sensitive interplay between three types of interactions, namely 1) the hard-sphere repulsion between particles in contact, 2) a combination of electrostatic repulsion due to the presence of surface charges on the nanoparticles and van der Waals attraction, and 3) the magnetic dipolar interaction due to the magnetite core of the particles. In the presence of the magnetic field the induced magnetic dipoles become attractive along the magnetic field. This in turn induces a shorter length scale along the field direction in comparison to the other two directions resulting in BCT symmetry. Particle polydispersity both in shape and size may also play some role in determining the c/a ratio.

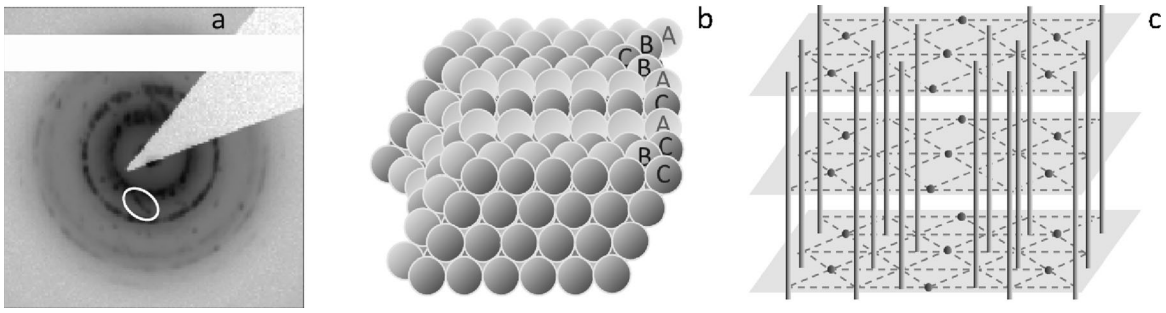

Figure 3. a) Diffraction pattern obtained after withdrawal of the magnetic field. Real space (b) and Fourier space (c) structures of a random hexagonal closed-packed (RHCP) lattice.

Interestingly, a re-examination of the capillary at the same height after the removal and overnight equilibration in the absence of magnetic field disclosed the formation of an entirely different crystal structure. Figure 3a shows the diffraction pattern of the new crystal at normal incidence in the absence of the magnetic field. This pattern consists of concentric rings around the beam stop and is characteristic for a powder of long-range-ordered self-organized crystals. The rings are not continuous but rather consist of reflections originating from different crystallites within the X-ray beam.

A careful inspection of the diffraction pattern shows a significant difference between the two lowest-order rings. In the outer ring the diffraction features appear at the same distance from the center of the diffraction pattern. In contrast, the diffraction intensity in the inner ring is spread over a range of q-values. Moreover, one can even see extended diffraction features such as the one marked by a circle in Figure 3a. These features are characteristic for colloidal crystals with a RHCP structure, which is illustrated in Figure 3b. The reciprocal lattice of this structure shown in Figure 3c consists of a number of sharp stacking-independent Bragg reflections and a set of the Bragg scattering rods that are induced by stacking disorder.[51,52] Depending on the crystal orientation, the Ewald sphere can cross the Bragg rods at different **Q**-values. Moreover, when an X-ray beam appears nearly parallel to the crystal planes, a piece of Bragg rod can become visible in the diffraction pattern as marked by the circle in Figure 3a.[47,48,52]

Colloidal spheres are known to self-organize into close-packed structures consisting of stacks of hexagonal close-packed planes. Periodic stacking of the planes in ABCABC or ABABAB sequences leads to the formation of FCC or hexagonal close-packed (HCP) structures, respectively. However, due to the fact that the free energy difference between these two structures[44–46] is quite small, spheres are often found to be stacked in a random mixture of these two particular stacking types.[47,49,50] Our results therefore show that the BCT crystals grown in the magnetic field transform to close-packed crystals with RHCP structure, which are often formed by hard colloidal spheres.

In conclusion, we have shown that external magnetic field stimulates core–shell magnetite/silica nanoparticles to self-assemble to a BCT crystalline structure. In the presence of the magnetic field each nanoparticle acquires an induced magnetic moment, which helps them to self-organize into a BCT lattice. However, in the absence of a magnetic field their self-organization is governed by the hard-sphere repulsion between the particles and a combination of electrostatic repulsion due to their charged surfaces and van der Waals attraction between them leading to the formation of a RHCP structure. Our findings are in good agreement with simulation results[39,40] on the assembly of these particles. However, our experimental study is remarkably different from that of simulation in one respect. The c/a ratio obtained from the experimental data is 15% different from that of touching spheres, which has not been predicted in simulations. Further theoretical and experimental studies are necessary to clarify the origin of this 15% change in the c/a ratio. This study allows us to determine a colloidal phase diagram, in which one can manipulate the crystalline phase and the lattice parameters of the colloidal crystal by external magnetic field.

Received: October 8, 2014
Published online: December 15, 2014

Keywords: colloidal crystals · core–shell nanoparticles · magnetic field · self-assembly · X-ray scattering

[1] J. H. Lee, Y. M. Huh, Y. W. Jun, J. W. Seo, J. T. Jang, H. T. Song, S. Kim, E. J. Cho, H. G. Yoon, J. S. Suh, J. Cheon, *Nat. Med.* **2007**, *13*, 95.
[2] M. Ye, Q. Zhang, Y. Hu, J. Ge, Z. Lu, L. He, Z. Chen, Y. Yin, *Chem. Eur. J.* **2010**, *16*, 6243.
[3] J. H. Lee, K. Lee, S. H. Moon, Y. Lee, T. G. Park, J. Cheon, *Angew. Chem. Int. Ed.* **2009**, *48*, 4174; *Angew. Chem.* **2009**, *121*, 4238.
[4] C. Xu, K. Xu, H. Gu, X. Zhong, Z. Guo, R. Zheng, X. Zhang, B. Xu, *J. Am. Chem. Soc.* **2004**, *126*, 3392.
[5] A. H. Lu, E. L. Salabas, F. Schüth, *Angew. Chem. Int. Ed.* **2007**, *46*, 1222; *Angew. Chem.* **2007**, *119*, 1242.
[6] X. Zhao, R. Tapec-Dytioco, K. Wang, W. Tan, *Anal. Chem.* **2003**, *75*, 3476.
[7] S. V. Sonti, A. Bose, *Colloids Surf. B* **1997**, *8*, 199.
[8] M. Klokkenburg, C. Vonk, E. M. Claesson, J. D. Meeldijk, B. H. Erné, A. P. Philipse, *J. Am. Chem. Soc.* **2004**, *126*, 16706.
[9] M. Klokkenburg, B. H. Erné, J. D. Meeldijk, A. Wiedenmann, A. V. Petukhov, R. P. A. Dullens, A. P. Philipse, *Phys. Rev. Lett.* **2006**, *97*, 185702.
[10] P. Krommenhoek, J. B. Tracy, *Part. Part. Syst. Charact.* **2013**, *30*, 759.
[11] K. Butter, P. H. H. Bomans, P. M. Frederik, G. J. Vroege, A. P. Philipse, *Nat. Mater.* **2003**, *2*, 88.

[12] J. H. J. Thijssen, A. V. Petukhov, D. C. 't Hart, A. Imhof, C. H. M. van der Werf, R. E. I. Schropp, A. van Blaaderen, *Adv. Mater.* **2006**, *18*, 1662.
[13] A. Yethiraj, A. van Blaaderen, *Nature* **2003**, *421*, 513.
[14] A. Yethiraj, A. Wouterse, B. Groh, A. van Blaaderen, *Phys. Rev. Lett.* **2004**, *92*, 058301.
[15] A. Yethiraj, J. H. J. Thijssen, A. Wouterse, A. van Blaaderen, *Adv. Mater.* **2004**, *16*, 596.
[16] X. L. Xu, G. Friedman, K. D. Humfeld, S. A. Majetich, S. A. Asher, *Adv. Mater.* **2001**, *13*, 1681.
[17] X. L. Xu, S. A. Majetich, S. A. Asher, *J. Am. Chem. Soc.* **2002**, *124*, 13864.
[18] M. Chorny, I. Fishbeina, B. B. Yellen, I. S. Alferieva, M. Bakaya, S. Gantac, R. Adamoa, M. Amijic, G. Friedmand, R. J. Levy, *Proc. Natl. Acad. Sci. USA* **2010**, *107*, 8346.
[19] Z. G. Forbes, B. B. Yellen, K. A. Barbee, G. Friedman, *IEEE Trans. Magn.* **2003**, *39*, 3372.
[20] K. H. Li, B. B. Yellen, *Appl. Phys. Lett.* **2010**, *97*, 083105.
[21] C. Ooi, R. M. Erb, B. B. Yellen, *J. Appl. Phys.* **2008**, *103*, 07E910.
[22] B. B. Yellen, G. Friedman, *J. Appl. Phys.* **2003**, *93*, 8447.
[23] B. B. Yellen, G. Friedman, *Langmuir* **2004**, *20*, 2553.
[24] B. B. Yellen, O. Hovorka, G. Friedmanet, *Proc. Natl. Acad. Sci. USA* **2005**, *102*, 8860.
[25] K. A. Mirica, S. T. Phillips, C. R. Mace, G. M. Whitesides, *J. Agric. Food Chem.* **2010**, *58*, 6565.
[26] K. A. Mirica, S. T. Phillips, S. S. Shevkoplyas, G. M. Whitesides, *J. Am. Chem. Soc.* **2008**, *130*, 17678.
[27] K. A. Mirica, S. S. Shevkoplyas, S. T. Phillips, M. Gupta, G. M. Whitesides, *J. Am. Chem. Soc.* **2009**, *131*, 10049.
[28] N. D. Shapiro, K. A. Mirica, S. Soh, S. T. Phillips, O. Taran, C. R. Mace, S. S. Shevkoplyas, G. M. Whitesides, *J. Am. Chem. Soc.* **2012**, *134*, 5637.
[29] J. Ge, Y. Hu, Y. Yin, *Angew. Chem. Int. Ed.* **2007**, *46*, 7428; *Angew. Chem.* **2007**, *119*, 7572.
[30] J. Ge, H. Lee, L. He, J. Kim, Z. Lu, H. Kim, J. Goebl, S. Kwon, Y. Yin, *J. Am. Chem. Soc.* **2009**, *131*, 15687.
[31] J. Ge, Y. D. Yin, *Adv. Mater.* **2008**, *20*, 3485.
[32] J. Ge, L. He, J. Goebl, Y. Yin, *J. Am. Chem. Soc.* **2009**, *131*, 3484.
[33] L. He, Y. Hu, X. Han, Y. Lu, Z. Lu, Y. Yin, *Langmuir* **2011**, *27*, 13444.
[34] J. Ge, Y. Yin, *J. Mater. Chem.* **2008**, *18*, 5041.
[35] J. Ge, J. Goebl, L. He, Z. Lu, Y. Yin, *Adv. Mater.* **2009**, *21*, 4259.
[36] M. Wang, L. He, Y. Hu, Y. Yin, *J. Mater. Chem. C* **2013**, *1*, 6151.
[37] R. Tao, J. M. Sun, *Phys. Rev. Lett.* **1991**, *67*, 398.
[38] B. Groh, S. Dietrich, *Phys. Rev. E* **2001**, *63*, 021203.
[39] A. P. Hynninen, M. Dijkstra, *Phys. Rev. E* **2005**, *72*, 051402.
[40] A. P. Hynninen, M. Dijkstra, *Phys. Rev. Lett.* **2005**, *94*, 138303.
[41] L. He, Y. Hu, H. Kim, J. Ge, S. Kwon, Y. Yin, *Nano Lett.* **2010**, *10*, 4708.
[42] V. Malik, A. V. Petukhov, L. He, Y. Yin, M. Schmidt, *Langmuir* **2012**, *28*, 14777.
[43] L. He, V. Malik, M. Wang, Y. Hu, F. E. Anson, Y. Yin, *Nanoscale* **2012**, *4*, 4438.
[44] P. G. Bolhuis, D. Frenkel, S. C. Mau, D. A. Huse, *Nature* **1997**, *388*, 235.
[45] A. Bruce, N. Wilding, G. Ackland, *Phys. Rev. Lett.* **1997**, *79*, 3002.
[46] S. Mau, D. Huse, *Phys. Rev. E* **1999**, *59*, 4396.
[47] I. P. Dolbnya, A. V. Petukhov, D. G. Aarts, G. J. Vroege, H. N. W. Lekkerkerker, *Europhys. Lett.* **2005**, *72*, 962.
[48] D. V. Byelov, J. Hilhorst, A. B. G. M. Leferink op Reinink, I. Snigireva, A. Snigirev, G. B. M. Vaughan, G. Portale, A. V. Petukhov, *Phase Transitions* **2010**, *83*, 107.
[49] J. Zhu, M. Li, R. Rogers, W. Meyer, R. Ottewill, W. Russell, P. Chaikin, *Nature* **1997**, *387*, 883.
[50] W. K. Kegel, J. K. G. Dhont, *J. Chem. Phys.* **2000**, *112*, 3431.
[51] H. Versmold, S. Musa, C. Dux, P. Lindner, *Langmuir* **1999**, *15*, 5065.
[52] A. V. Petukhov, I. P. Dolbnya, D. G. A. L. Aarts, G. J. Vroege, H. N. W. Lekkerkerker, *Phys. Rev. Lett.* **2003**, *90*, 028304.

